International Journal of Multiphase Flow 39 (2012) 29–36

Contents lists available at SciVerse ScienceDirect

International Journal of Multiphase Flow

journal homepage: www.elsevier.com/locate/ijmulflow

Droplet breakup and viscosity-stratified flows in microchannels

Thomas Cubaud *, Bibin M. Jose, Samira Darvishi, Ruopeng Sun

Department of Mechanical Engineering, Stony Brook University, Stony Brook, NY 11794, USA

ARTICLE INFO

Article history:
Received 9 August 2011
Received in revised form 18 October 2011
Accepted 26 October 2011
Available online 3 November 2011

Keywords:
Droplet
Stratifications
Viscous displacement
Fingering
Plume
Microfluidics

ABSTRACT

The hydrodynamic coupling between droplets and viscous stratifications is examined in square microchannels. A segmented flow of droplets is injected into a viscosity-stratified flow region. The large difference in velocity between parallel streams having dissimilar viscosities produces a variety of droplet dynamics, including breakup into an array of daughter droplets. We characterize stable viscous stratifications generated using hydrodynamic focusing into a square microchannel and we present a general phase-diagram of droplet behavior. The capillary number is shown to influence both the morphology and dynamics of daughter droplets. In particular, the film thickness between droplets and walls is measured along with the droplet velocity. Deformable droplets significantly disrupt viscous stratifications at low Reynolds numbers and a plume is produced in the trail of the last daughter droplet. The formation and evolution of viscous fingers from the edges of high-viscosity stratifications are discussed. This study shows the possibility to displace high-viscosity oil with droplets in microgeometries.

1. Introduction

Multiphase flows in microfluidic platforms have attracted much attention in recent years due to a wide range of applications (Squires and Quake, 2005; Günther and Jensen, 2006; Tabeling, 2005; Guillot et al., 2006). The laminar property of microflows is useful for structuring streams and the combination of microgeometries and fluid injections allows for manipulating complex sequences of events. Microfluidic droplets constitute the elementary building blocks of emulsions and offer well-controlled vessels for enclosing and transporting microreactions (Song et al., 2006; Teh et al., 2008; Christopher and Anna, 2007; Brouzes et al., 2009; Baroud et al., 2010). Recent developments have shown the possibility to generate multiple-emulsions where diverse droplets are sequestered inside larger droplets (Seo et al., 2007; Wan et al., 2008; Pannacci et al., 2008; Köster et al., 2008; Wang et al., 2011). Continuous-flow-based methods for micro-manipulating droplets include geometrically induced breakup at T-junctions (Link et al., 2004; Ménétrier-Deremble and Tabeling, 2006; Leshansky and Pismen, 2009) and breakup with focusing sections (Prat et al., 2006; Cubaud, 2009; Che et al., 2011). Better understanding the underlying principles governing the dynamic response of droplets to external microflows is of both fundamental and practical interests. In particular, modifying the physicochemical environment of microfluidic droplets is a key step in the development of new methods for processing on-demand soft materials.

Multiphase flows are classified into two broad categories: (a) dispersed flows, and (b) separated flows (Crowe, 2006). In dispersed microflows, fluids are typically distributed along the flow direction and form alternated fluid segments. For instance, immiscible fluids tend to adopt the configuration of elongated droplets separated by continuous liquid plugs. By contrast, separated microflows involve phases that are structured normal to the flow direction. In stratified flows, the interface between miscible fluids is generally aligned with the microchannel axis.

Stratified microflows have received considerable interest for their ability to generate a variety of concentration gradients (Ismagilov et al., 2000; Irimia et al., 2006). In turn, the destabilization and recombination of parallel flows enhance fluid micromixing (Nguyen and Wereley, 2006; Neils et al., 2004; Aubin et al., 2010; Lee et al., 2011). A common technique used for generating parallel flows consists in focusing a central sample stream within a sheath fluid injected from side-channels (Knight et al., 1998; Lee et al., 2006; Wu and Nguyen, 2005; Larsen and Shapley, 2007). For fluids having a large difference in viscosity, previous studies showed the possibility to form lubricated threads when the more viscous liquid is injected into the central channel (Cubaud and Mason, 2006) or viscosity-stratified flows when the highly viscous fluid is injected into the side-channels (Cubaud and Mason, 2008b). In the latter case, parallel fluid layers exhibit a large difference in velocity with a fast central stream and a slow sheath flow.

Here, we inject a segmented flow of droplets into a viscous-stratified flow using two consecutive hydrodynamic focusing

* Corresponding author. Address: 113 Light Engineering Building, Stony Brook University, Stony Brook, NY 11794, USA. Tel.: +1 631 632 9431; fax: +1 631 632 8544.
E-mail address: thomas.cubaud@stonybrook.edu (T. Cubaud).

0301-9322/$ - see front matter © 2011 Elsevier Ltd. All rights reserved.
doi:10.1016/j.ijmultiphaseflow.2011.10.011

sections. We investigate the interrelation between droplet dynamics and streams having different velocities in a compact microchannel. First, focus is on the deformation and breakup of a "mother" droplet into a variety of "daughter" droplets. We characterize stable viscous stratifications produced using hydrodynamic focusing into a square microchannel. The role of the viscosity contrast between separated flows on droplet breakup is demonstrated and a general phase-diagram of droplet behavior is presented. The capillary number is shown to influence both the morphology and dynamics of daughter droplets. In particular, the film thickness between droplets and walls is measured and the droplet speed is compared with theoretical models.

Second, the alteration of viscous strata is examined. We show that droplets significantly disturb viscous layers at low Reynolds numbers. The closing of viscous stratifications in front of the droplet and the resulting high-viscosity fluid displacement is reported. The difference in velocity between droplets and stratifications produces a slow moving plume in the trail of the last daughter droplet. The plume is characterized by the evolution of two fingers stretched from the high-viscosity matrices and dragged into the central stream. The initial plume size is measured as a function of fluid properties and flow parameters. Finally, we discuss the dynamics of small droplets confined between streams having a very large viscosity contrast and acting as "soft walls".

2. Material and methods

The flow geometry consists of two hydrodynamic focusing junctions connected in series (Fig. 1). The microfluidic device is made of glass and silicon. All channels are square in cross-section and have identical height $h = 250$ μm. The initial or "mother" droplets are generated in the first junction by steadily injecting the disperse phase ($L1$) in the central channel with a volumetric flow rate Q_1 and by symmetrically introducing the low-viscosity continuous phase ($L2$) from the side-channels with a total volumetric flow rate Q_2. Adjusting the flow rates Q_1 and Q_2 allows for controlling the mother droplet size d_0 with the initial flow rate ratio $\varphi_0 = Q_1/Q_2$ as well as the average inlet flow velocity carrying the droplets $J_D \approx (Q_1 + Q_2)/h^2$. The high-viscosity continuous phase ($L3$) is continuously introduced in the second junction with a total flow rate Q_3. This method produces parallel viscous stratifications composed of a low-viscosity central stream of width ε ensheathed between two high-viscosity streams. For a given fluid selection ($L1$, $L2$, $L3$), the width ε is adjusted with flow rate ratio $\varphi = (Q_1 + Q_2)/Q_3 \approx J_D/J_S$, where $J_S = Q_3/h^2$ is the superficial velocity of the viscous stratifications. Upon entering the parallel streams region, a mother droplet can breakup into an array of "daughter" droplets. The number of daughter droplets is labeled with the index n. In turn, the velocity differential between droplets and stratifications leads to the closure of stratifications in the front of the droplets and the formation of a plume (or wake) at the rear of the last daughter droplet (Fig. 1).

Droplets are made of pure DI water and both external phases are composed of silicone oils having various viscosities. The low and high-viscosity oils are miscible and chosen to examine the effect of the viscosity contrast between parallel streams. The Péclet number associated with these miscible flows is large and diffusion effects are neglected. To focus on the influence of the viscosity on strata, we have fixed $\eta_1 = 1$ cP and $\eta_2 = 4.6$ cP and varied $\eta_3 = 4.6$, 48, 486, and 4865 cP. Therefore, the system is characterized by $\eta_1 < \eta_2 \leqslant \eta_3$, with a constant viscosity ratio $\chi_0 = \eta_1/\eta_2 = 0.22$ for the initial segmented flow and four different viscosity ratios $\chi = \eta_2/\eta_3 = 1$, 1/10, 1/105, and 1/1057 between the low-viscosity ($L2$) and the high-viscosity fluid ($L3$). Over the range of silicone oils used in this study, the interfacial tension between silicone oil and water is measured as $\gamma_{12} \approx \gamma_{13} \approx 41$ mN/m. When immersed in a bath of silicone oil, the static contact angle of water on glass is measured using a goniometer and found relatively large $\theta_S \approx 110°$. However, the advancing contact angle $\theta_A \to 180°$ for small capillary numbers, $Ca \geqslant 10^{-3}$, where $Ca = \eta V/\gamma_{12}$, with η being the viscosity of the oil and V the speed of the contact line. Since mother droplets are injected at relatively low speed in the low viscosity oil ($L2$), we observe the dewetting of $L2$ between the walls and the droplet in the "dispersed flow region" (Fig. 1). However, in general, dynamic wetting phenomena do not significantly influence our system.

3. Structure of stratifications

We first examine the morphology of unperturbed stratifications between $L2$ and $L3$. The stability of viscosity-stratified flows has been examined in the axisymmetric pipe (Hickox, 1971; Cao et al., 2003, 2004; d'Ocle et al., 2008; Selvam et al., 2007) and plane (Yih, 1967; Yiantsios and Higgins, 1988; Gondret and Rabaud, 1997) flow configurations but less is known for square microchannels. Here, the Reynolds number associated with the flow is small and inertial effects are neglected. The base flow consists of parabolic profiles in each layer (Fig. 2a). During the period of time between each incoming droplet, viscous stratifications are observed to "heal" and the width of the low-viscosity stream ε remains constant in the observation channel. For a given viscosity contrast $\chi = \eta_2/\eta_3$, the width ε depends on the flow rate ratio between the central and the sheath streams $\varphi = (Q_1 + Q_2)/Q_3$. For hydrodynamic focusing in plane geometries (Cubaud and Mason, 2008b), the width of central stream ε can be analytically deduced assuming continuity of the tangential stress at the fluid interface according

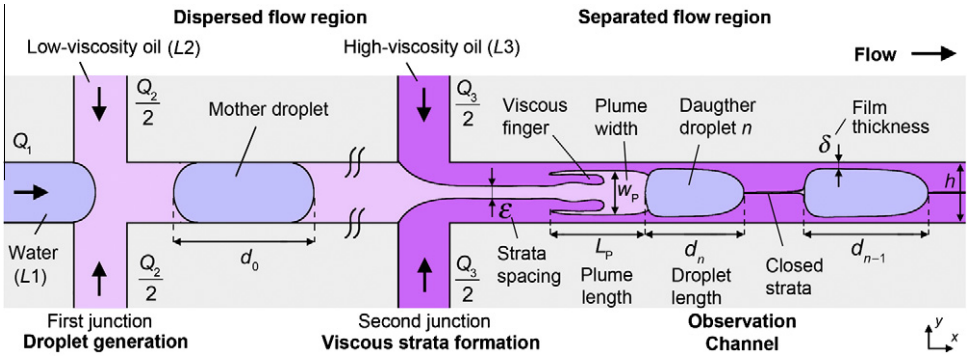

Fig. 1. Schematics of the microflow geometry with a two-step hydrodynamic focusing section. Droplets are formed in the first section and viscous stratifications are introduced in the second section (see text for details).

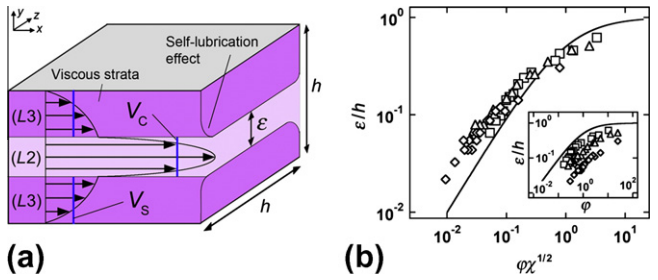

Fig. 2. (a) Sketch of the velocity profile of viscous stratified flows in a square microchannel where V_C is the average velocity of the central stream and V_S is the average velocity of stratifications. (b) Evolution of the normalized central stream width ε/h as a function of the flow rate ratio $\varphi = (Q_1 + Q_2)/Q_3$ and the viscosity ratio $\chi = \eta_2/\eta_3 = 1/10$ (△), 1/105 (□), and 1/1057 (◇). Solid line: $\varepsilon/h = [1 + (\varphi\chi^{1/2})^{-1}]^{-1}$. Inset shows normalized central stream width ε/h as a function of φ.

to $\varepsilon/h \approx [1 + (\varphi\chi)^{-1}]^{-1}$. In square microchannels, a previous study (Cubaud and Mason, 2007) showed that when central and sheath streams have identical viscosity (i.e., $\chi = 1$), the width ε follows the plane geometry approximation: $\varepsilon/h \approx (1 + \varphi^{-1})^{-1}$. Here, we measure ε as a function of φ for three viscosity ratios $\chi \approx 1/10$, 1/105, and 1/1057 (Fig. 2b – inset). As expected, the widths ε corresponding to different χ do not collapse on a single curve. We also find that, on the contrary to the plane geometry configuration, the width of the central stream ε does not scale with the viscous stress ratio parameter $\varphi\chi$. However, the morphology of viscous-stratified flows in square microchannel is characterized by $\varepsilon < h$ (Fig. 2a) and suggests an analogy with the 2D free-shear layer problem of parallel streams of different viscosities (Batchelor, 1967). In this case, similarity variables can be used for the stress condition at the interface and, for fluids having similar densities, the thickness of the transition layer depends on the ratios $\chi^{1/2}$ and U_A/U_B, where U_A and U_B are the uniform velocities of each stream far away from the transition. This scaling for the viscosity parameter $\chi^{1/2}$ was used in this work and data for ε collapse into a single curve when plotted as a function of $\varphi\chi^{1/2}$ (Fig. 2b). In particular, we find that the central stream width can be estimated with $\varepsilon/h \approx [1 + (\varphi\chi^{1/2})^{-1}]^{-1}$. This approximation is also in good agreement with the case $\chi = 1$ since the equation $\varepsilon/h \approx (1 + \varphi^{-1})^{-1}$ is recovered for viscosity-matching streams. Another aspect of parallel flows having a large difference in viscosity is the tendency for low-viscosity fluids to migrate toward the region of high shear (Yu and Sparrow, 1969; Than et al., 1987; Cubaud and Mason, 2009). The "self-lubrication" property yields a small curvature of the miscible fluids interface between $L2$ and $L3$ and the measured widths ε slightly surpass our empirical correlation for $\varepsilon/h \ll 1$ (Fig. 2).

When the side streams have a large viscosity ($\chi \ll 1$), the central stream moves at a significantly larger velocity compared to the sheath streams. The average velocity of the central stream is denoted by $V_C \approx (Q_1 + Q_2)/(h\varepsilon)$ and the average speed of the sheath flow can be written as $V_S \approx Q_3/[h(h - \varepsilon)]$. The experimental correlation for ε allows us to estimate the effective slip ratio between the two parallel phases according $V_C/V_S \sim \varphi + \chi^{-1/2}$ when $\varepsilon/h \ll 1$. This heterogeneous flow field has a strong effect on droplet dynamics.

4. Droplets

4.1. Conditions for breakup

A droplet entering the viscosity-stratified field typically experiences a deformation of its front end-cap. The droplet nose first becomes elongated due to the additional viscous stresses caused by the side flow. If the deformation of the front end-cap is large enough, a neck appears along the droplet core and capillary forces induce breakup to reduce interfacial area. For long droplets ($d_0/h \gg 1$), this mechanism can repeat itself on the remaining initial droplet volume and, eventually, a mother droplet can breakup into an array of n smaller daughter droplets.

In a similar flow configuration (i.e., two focusing sections in series) but in the absence of viscous stratifications ($\eta_2 = \eta_3$), previous work (Cubaud, 2009) identified three regimes of droplet behavior: (a) relaxing deformation for small Q_3, (b) convective breakup for moderate Q_3, and (c) absolute breakup for large Q_3. The term convective breakup refers to a droplet splitting mechanism that occurs downstream from the junction and the term absolute breakup corresponds to a droplet fragmentation process localized at the junction, similar to the dripping regime (Cubaud and Mason, 2008a). The convective breakup regime was not observed here given the small droplet viscosity ($\eta_1 = 1$ cP). We find that for strictly identical flow rates (Q_1 and Q_2 for the droplet generation and Q_3 for the side flow), increasing the viscosity of stratifications η_3 produces a larger number n of daughter droplets (Fig. 3). Although different plateaus of fixed n are found as Q_3 increases, overall, the number of daughter droplets n appears to be roughly proportional to the side flow rate Q_3. In order to conserve the mass of the initial droplet, the typical size of daughter droplets decreases with n. In this example, the mother droplet length d_0 is measured between the tips of the two end-caps (Fig. 1) and remains approximately constant $d_0/h \approx 3.4$. The size of initial droplet d_0, however, has a highly non-linear effect on deformation and breakup mechanisms.

The presence of viscous stratifications at the second junction effectively changes the environment of droplets. In particular, the sharp increase in the viscosity of the external phase modifies the ratio of capillary to viscous stresses exerted at the droplet interface and triggers a variety of dynamics. To account for this effect, we define the capillary number associated with the side-flow based on the superficial velocity of $L3$ by $Ca_3 = \eta_3 Q_3/(\gamma_{13} h^2)$. For a fixed inlet flow (constant Q_1 and Q_2), droplets deform for small Ca_3 and breakup for large Ca_3. The droplet dynamic response also depends on the relative change of Ca_3 compared to the inlet flow. For instance, if Ca_3 is fixed, a change in Q_1 and Q_2 will yield different transitions between droplet regimes. To quantify this relative

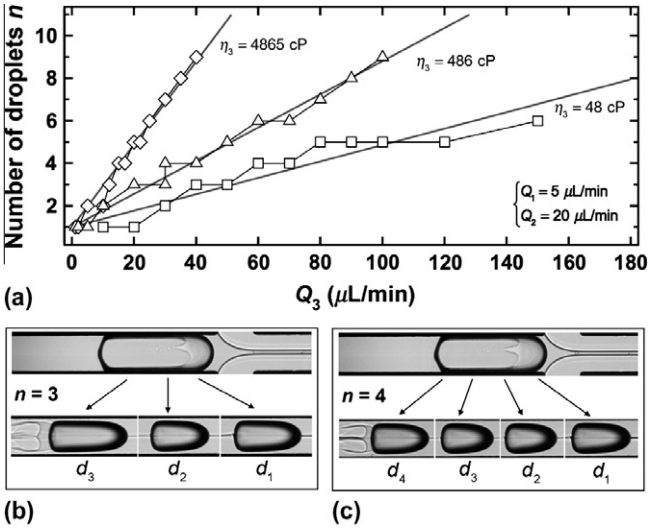

Fig. 3. Evolution of the number of daughter droplets n for fixed inlet flow rates ($Q_1 = 5$ and $Q_2 = 20$ μl/min) and increasing stratification volume flow rate Q_3, viscosity ratios $\chi = 1/10$ (△), 1/105 (□), and 1/1057 (◇). (b) Droplet breakup with three daughter droplets ($n = 3$), $Q_3 = 30$ μl/min ($\chi = 1/105$). (c) Droplet breakup with four daughter droplets ($n = 4$), $Q_3 = 40$ μl/min ($\chi = 1/105$).

change, a useful dimensionless quantity is the homogeneous side-flow volume fraction $\alpha_3 = Q_3/(Q_1 + Q_2 + Q_3)$. The parameter $\alpha_3 Ca_3$ was previously used to locate droplet deformation regimes on a phase-diagram in the absence of viscous stratifications ($\eta_2 = \eta_3$) (Cubaud, 2009). In a similar fashion, we find here that for a given viscosity ratio χ, droplet regimes can be located on a phase-diagram where d_0/h is plotted as function of $\alpha_3 Ca_3$. However, when data collected for the four viscosity ratios ($\chi = 1$, 1/10, 1/105, and 1/1057) are plotted together on the same phase diagram, the breakup/non-breakup transition lines are shifted for each χ. Indeed, the viscosity contrasts between the external phases plays an important role in the stratification morphologies. Our study of the central width ε indicates that the quantity $\chi^{1/2}$ is relevant in this system. We find empirically that transition lines are superimposed when the viscosity contrast between parallel streams is taken into account with the dimensionless quantity $\alpha_3 Ca_3 \chi^{1/2}$. This quantity is interpreted as a modified capillary number $Ca_M = \eta_M V_M/\gamma_{12}$, where the effective viscosity $\eta_M = (\eta_2\eta_3)^{1/2}$ is the geometric mean of the carrier viscosities and $V_M = (Q_3/h^2)[Q_3/(Q_1 + Q_2 + Q_3)]$ is the superficial velocity of $L3$ weighted by its homogeneous volume fraction α_3. When data for all χ are plotted together, breakup and non-breakup regimes are located on each side of a clear separation curve defined by $d_0/h = aCa_M^{-b}$, with $a = 0.58$ and $b = 0.3$ (Fig. 4). In the absence of viscous stratifications ($\chi = 1$), we retrieve the original parameter $\alpha_3 Ca_3$ and find very good quantitative agreement with previous work on high-viscosity droplets. In this work, the droplet viscosity η_1 was not varied since previous results showed that η_1 does not significantly influence breakup process. These results also highlight the non-linear dependency of droplet size d_0 on breakup mechanism in strongly bounded flows with an imposed length scale h. In general, breaking smaller droplets is difficult due to the necessary large deformation of the end cap curvature. Here, to focus on breakup dynamics, experiments were conducted with relatively large droplets $d_0/h \geqslant 2$. In summary, we find that the dimensionless quantity $Ca_M = \alpha_3 Ca_3 \chi^{1/2} = Q_3^2(\eta_2\eta_3)^{1/2}/[\gamma_{12}(Q_1 + Q_2 + Q_3)h^2]$ is very useful to locate droplet regimes. Once droplets are produced, however, the main capillary number based on the multiphase flow superficial velocity and the stratification viscosity η_3, $Ca = \eta_3(Q_1 + Q_2 + Q_3)/(h^2\gamma_{13})$, is more relevant. The use of this capillary number in the observation channel is justified by the fact that droplets are almost entirely surrounded by the more viscous fluids $L3$ while being carried away at near the average multi-component flow velocity.

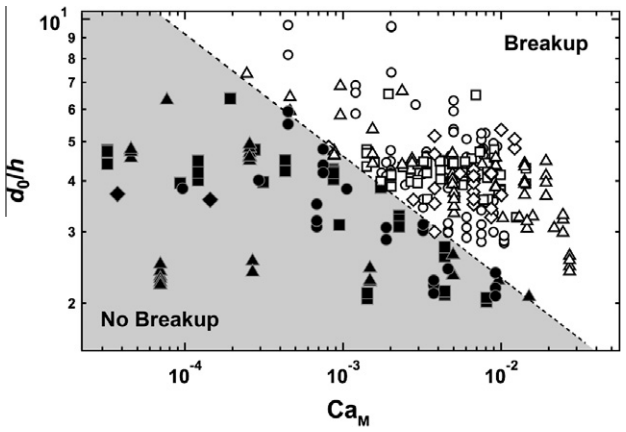

Fig. 4. Phase diagram of droplet breakup in viscous stratifications. Normalized size of mother droplet d_0/h versus modified capillary number $Ca_M = (\eta_2\eta_3)^{1/2}Q_3^2/[(Q_1 + Q_2 + Q_3)h^2\gamma_{12}]$. Filled symbols: no breakup ($n = 1$), open symbols: breakup ($n \geqslant 2$). Viscosity ratio: $\chi = 1$ (○), 1/10 (△), 1/105 (□), and 1/1057 (◇). Dashed line: $d_0/h = 0.58Ca_M^{-0.3}$.

4.2. Daughter droplet size

For $n \geqslant 3$, the length of the first daughter droplet d_1 is measured from the micrographs and found to increase with the flow rate ratio $\varphi = (Q_1 + Q_2)/Q_3$ (Fig. 5a). For the asymptotic regime associated with very small viscosity ratios ($\chi \leqslant 1/10$), the normalized droplet size d_1/h follows a scaling that is independent from χ according to $d_1/h = a\varphi^{0.66}$ with $a = 2.7$ (Fig. 5a). For viscosity ratios χ near unity ($\eta_2 \sim \eta_3$), the previous scaling underestimates the droplet size d_1. Further experimental and theoretical work is required to better understand droplet breakup in this regime. The behavior for $\chi \ll 1$, however, is in good qualitative agreement with the scaling of gas bubbles and liquid droplets found in the flow-focusing literature (Gañán-Calvo, 1998). We also show that the intrinsic ratio d_1/L_1, where L_1 is the length of the liquid plug between the first and the second droplet, is directly proportional to the flow rate ratio according to $d_1/L_1 = a\varphi$ with $a = 1.5$ (Fig. 5b).

As the capillary number Ca increases, the film thickness δ between the droplet and the walls grows and droplets become slender. Although the volume of the first droplet decreases with Ca, its length d_1 is found to remain relatively independent from Ca. This property is not conserved for the length of the second droplet d_2. Indeed, after the first breakup, the front end-cap of the remaining mother droplet is already deformed due to the large capillary number in the observation channel and the length of the second droplet d_2 is typically smaller than d_1. For a large number of daughter droplets, $n \geqslant 4$, data show that the size ratio $\Gamma = d_2/d_1$ decreases with Ca according to $\Gamma = 1 - aCa^{0.5}$, with $a = 0.22$ (Fig. 5c). In this graph, data points for different viscosity ratio χ are distributed in different regions of the capillary number Ca as the stratification viscosity η_3 varies. The length of the following droplets (d_3, d_4,...) are very similar to d_2. This property holds until the last two droplets (d_{n-1} and d_n), which are usually adjusted by the

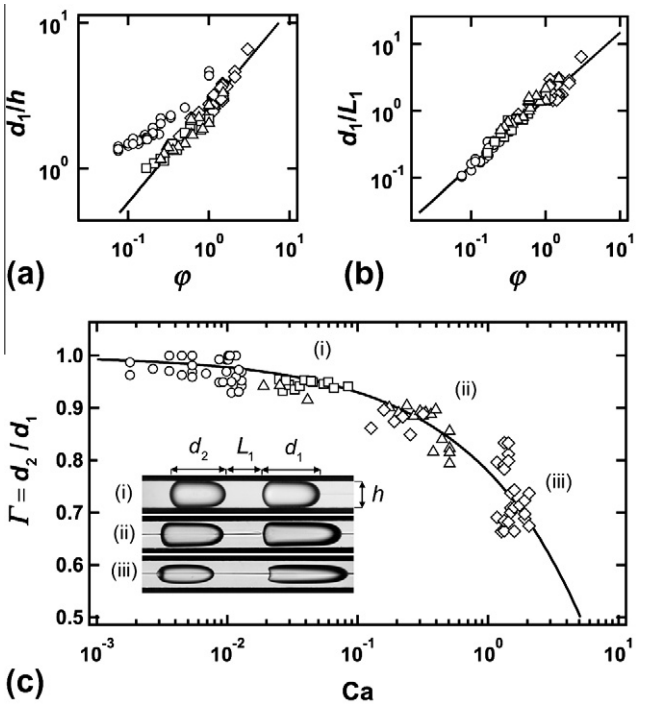

Fig. 5. Evolution of daughter droplet size. Viscosity ratios: $\chi = 1$ (○), 1/10 (△), 1/105 (□), and 1/1057 (◇). (a) Size of the first daughter droplet d_1 as a function of the flow rate ratio φ. Solid line: $d_1/h = 2.7\varphi^{0.66}$. (b) Aspect ratio of daughter droplet segmented flows d_1/L_1 versus flow rate ratio φ. Solid line: $d_1/L_1 = 1.5\varphi$. (c) Aspect ratio between the second and first daughter droplets $\Gamma = d_1/d_2$ versus the capillary number Ca. Solid line: $\Gamma = 1 - 0.22Ca^{0.5}$.

stratified system to "swallow" the remains of the mother droplet. The size reduction after the first breakup was also observed in a similar system when droplet breakup is induced by velocity difference between inlet and side flows (Che et al., 2011). Overall, this mechanism introduces polydispersity in the resulting droplet population.

4.3. Droplet dynamics

For large capillary numbers Ca, droplets are significantly distorted by viscous stresses and adopt a characteristic bullet-shape with a large curvature at the droplet front and a nearly flat bottom. The film thickness δ between the sidewalls and the center of large droplets ($d > 2h$) is measured from micrographs as a function of Ca in the observation channel (Fig. 6a). For low $Ca < 10^{-2}$, the film thickness is very small and cannot be directly determined using our system so we assume $\delta \approx 0$. For very low $Ca \sim 10^{-3}$, the film breaking is revealed by the presence of wetting contact lines between the droplet and the walls. Overall, we find that data are well fit with the function $\delta/h = aCa^{2/3}$, with $a = 0.11$. The exponent 2/3 is given by lubrication approximation for thin films and is consistent with previous experimental and theoretical results on the motion of bubbles in circular and polygonal capillaries (Bertherton, 1961; Ratulowski and Chang, 1989; Wong et al., 1995).

The droplet velocity V_D in the viscous stratifications is measured from high-speed movies and compared with the superficial multiphase flow velocity $J = (Q_1 + Q_2 + Q_3)/h^2$ as a function of the capillary number Ca (Fig. 6b). For small $Ca < 10^{-2}$, the film thickness is negligible and as expected the velocity ratio $V_D/J \approx 1$. For larger value of Ca, the droplet velocity rises compared to the average superficial velocity with $V_D/J \approx 2$ for capillary numbers Ca near unity. Similar to the motion of long bubbles in circular tubes (Bertherton, 1961), data can be described with a power law based on the capillary number with an exponent 2/3. In particular, we find that data points collapse on a single curve that can be fit with the function $V_D/J = 1 + aCa^{2/3}$ with $a = 1.1$. We conclude that droplet speed can be approximated by $V_D \sim J$, which shows that this dynamical system self-adapts and regulates flow to maintain a steady droplet velocity. This property has major implications on the dynamics of miscible viscous stratifications since the central stream velocity $V_C > J$ and the stratifications average velocity $V_S < J$.

5. Alteration of viscous stratifications

5.1. Closure of front stratifications

We examine the deformation of stratifications due to the presence of a translating droplet. The velocity difference between droplets and strata has a variety of effects on flow morphologies. In

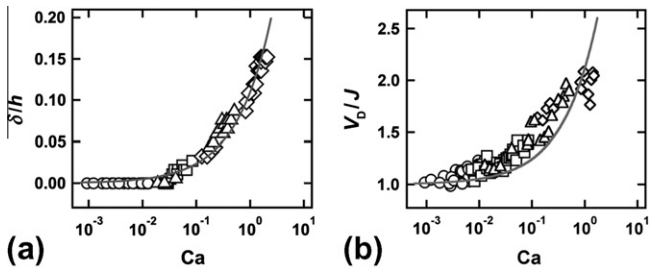

Fig. 6. Influence of capillary number Ca on film thickness and droplet speed. Viscosity ratio: $\chi = 1$ (○), 1/10 (△), 1/105 (□), and 1/1057 (◇). (a) Evolution of the film thickness δ as a function of the capillary number Ca for large droplets $d > h$, solid line: $\delta/h = 0.11Ca^{2/3}$. (b) Evolution of the normalized droplet speed V_D/J as a function of capillary number Ca, solid line: $V_D/J = 1 + 1.1Ca^{2/3}$.

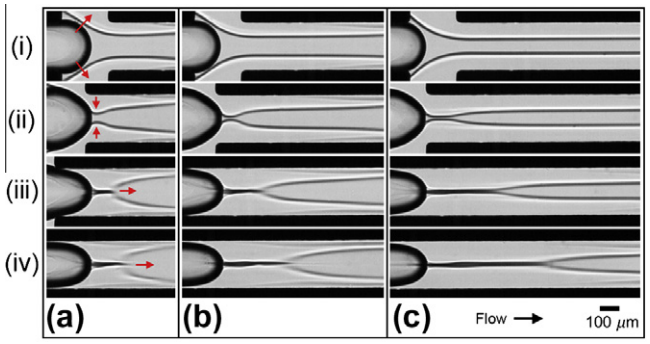

Fig. 7. Initial stages of droplet ingestion. Time-series in the reference frame of the droplet front: (i) droplet entering a steady viscous-stratified flow, (ii) strata displacement and formation of a pinching neck (iii) propagation of closure front, and (iv) zipping mechanism downstream from the droplet. Viscosity contrast $\chi = 1/105$, flow rates in μl/min, $Q_1 = 5$, $Q_2 = 20$, and $Q_3 = 1$ (a), 2 (b), and 10 (c).

particular, since the droplet velocity V_D is larger than the average stratification velocity V_S, the droplet displaces the high-viscosity fluid $L3$ into the central stream. This effect causes the closing of strata in front of the droplet. Fig. 7 displays the successive stages of a droplet entering a viscous-stratified flow in the reference frame of the droplet nose. The droplet emission frequency is chosen low to give enough time for strata to repair between each droplet and the spacing ε between layers is initially constant. The first stage corresponds to the displacement of $L3$ in the second junction (Fig. 7i). As the droplet progresses inside the microchannel, the droplet nose elongates to accommodate for the new viscous environment and two symmetrical bulges grow from the high-viscosity layers into the central stream (Fig. 7ii). These bulges are fed by the displaced liquid $L3$ and form a pinching neck in front of the droplet. The neck develops into a front that effectively closes the stratifications (i.e., $\varepsilon \to 0$) ahead of the droplet (Fig. 7iii). The closure front then propagates faster than the droplet suggesting a zipping mechanism (Fig. 7iv). The solid-like behavior of this propagation front is interpreted as being due to the large viscosity coefficient η_3 of stratifications, which overall facilitates the diffusion of momentum (Guyon et al., 2001). This process suggests an analogy with an ingestion mechanism and locally produces a high-viscosity surrounding for the first droplet. We observe that stratifications between each following daughter droplet are also closed and droplets are nearly entirely enveloped with the high-viscosity fluid $L3$.

5.2. Plume formation and evolution

A viscous plume is observed in the trail of the last droplet (Fig. 8a). After the final droplet passes the source of injection of the more viscous oil (i.e., second junction), stratifications progressively recover their initial morphology. In the process, the distance between strata ε decreases and the transition region between plume and steady stratifications is slowly convected at a speed on the order of V_S. As $L2$ enters the viscous constriction, the fluid experiences a convective acceleration until the average velocity reaches $V_C \approx Q_1/(\varepsilon h)$. Since for $\chi \ll 1$, the central stream average velocity is much greater than the stratifications velocity, $V_C \gg V_S$, the fluid $L2$ progressively fills a cavity between droplet and strata, which leads to the formation of a plume. The plume evolution is characterized by the formation and propagation of two viscous fingers. We define the initial plume size L_{P0} when the strata front inverses curvature due to the drag exerted on its edges by the fast flowing central stream (Fig. 8a – bottom). The plume is defined between the source of the fingers in the high-viscosity matrix and the back of the droplet. We measure the size of the initial plume L_{P0} for

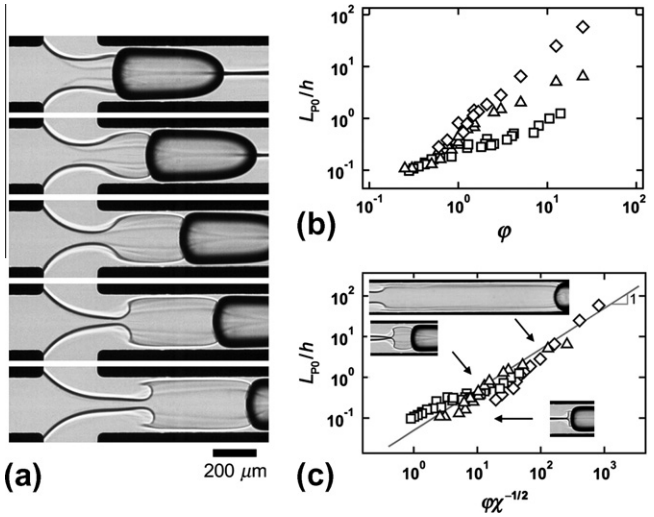

Fig. 8. Plume formation in the trail of the last droplet translating in stratifications. (a) Time-series of the "swallowing" of a droplet leading to plume formation, $\Delta t = 10$ ms, viscosity contrast $\chi = 1/105$, flow rates in μl/min, $Q_1 = 5$, $Q_2 = 20$, and $Q_3 = 10$. (b) Evolution of the normalized initial plume length L_{P0}/h as a function of flow rate ratio φ. (c) Dimensionless plume length L_{P0}/h versus $\varphi\chi^{-1/2}$, solid line: $L_{P0}/h = 0.05\varphi\chi^{-1/2}$.

the small three viscosity contrasts χ as a function of the flow rate ratio φ (Fig. 8b). This phenomenon is relatively complex and the volume of the initial plume $Vol_0 \sim (h - 2\delta)^2 L_{P0}$ is determined during the closing of back stratifications. Although, L_{P0} increases with the flow rate ratio φ, we also expect L_{P0} to be proportional to the viscosity parameter $\chi^{-1/2}$ since our scaling analysis suggests that the slip ratio of compact viscosity-stratified microflows depends on both φ and $\chi^{-1/2}$. Here, we empirically find that the initial plume length L_{P0} is linearly proportional with the dimensionless quantity $\varphi\chi^{-1/2}$ according to $L_{P0}/h = a\varphi\chi^{-1/2}$, with $a = 0.05$ (Fig. 8c).

We examine the temporal evolution of the positions of the droplet rear and plume along the observation channel (Fig. 9a). The time is set to zero when the plume is fully developed, i.e., at the moment when fingers emerge from the strata edges ($L_P = L_{P0}$). The linear evolution of these structures indicates a constant velocity for both the droplet $V_D = x_D/t$ and the plume, which is assumed to travel at the average stratification speed with $V_S = x_P/t$. Since $V_D > V_S$, the plume length L_P grows over time according to $L_P = L_{P0} + (V_D - V_S)t$. The velocity ratio V_D/V_S between the droplet rear and the plume is measured as a function of the injection flow

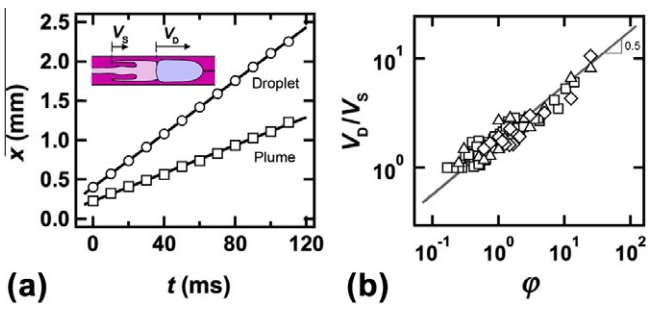

Fig. 9. Relative evolution of plume and droplet. (a) Temporal evolution of the positions of the droplet rear (○) and the plume (□), viscosity contrast $\chi = 1/105$, flow rates in μl/min, $Q_1 = 5$, $Q_2 = 20$, and $Q_3 = 20$. (b) Droplet-to-plume velocity ratio, V_D/V_S, as a function of flow rate ratio φ, viscosity ratio: $\chi = 1/10$ (△), 1/105 (□), and 1/1057 (◇). Solid line: $V_D/V_S = 1.8\varphi^{0.5}$.

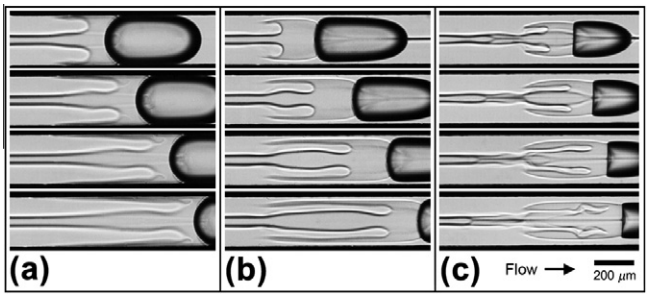

Fig. 10. Influence of film thickness δ on plume morphology and viscous fingers. Time-series in the reference frame of the back of the plume, viscosity ratio $\chi = 1/105$, (a) for $\delta \approx 0$, stratifications fully detach from the side-walls ($\varphi = 1.5$, $Ca \approx 2 \times 10^{-3}$), (b) for low value of δ, droplets detach stratifications from the top and bottom walls at their rear ($\varphi = 1.25$, $Ca \approx 1.4 \times 10^{-2}$), and (c) for moderate value of δ, the droplet create a cavity ($\varphi = 1.5$, $Ca \approx 4.4 \times 10^{-2}$).

rate ratio φ (Fig. 9b). For a viscosity contrast χ spanning over two decades, data collapse onto a single curve that is well fit with the scaling $V_D/V_S = a\varphi^{0.5}$, with $a = 1.8$. This finding is in good agreement with the observation of wide plumes for relatively large flow rate ratios φ (and large spacing between strata ε) and small plumes for small flow rate ratio $\varphi < 1$. Further work is required to elucidate the independence of the velocity ratio V_D/V_S from the viscosity contrast χ. The morphology of the transition region between plume and steady stratifications, however, evolves along the flow direction and partial lubrication phenomena are revealed by the presence of viscous fingers.

The plume morphology is rather intricate with the propagation of lubricated fingers in the center (Fig. 10). The fingers are stretched from the high-viscosity streams and advected by the low-viscosity fluid near V_C. Given the large difference in viscosity between the fluids, fingers flow faster than the back of the plume and, eventually, they close in on the droplet. Since the initial plume morphology vaguely resembles a mushroom cloud, we have opted for the term "plume" to describe the droplet wake in the viscous stratifications. Fig. 10 displays time-series of the fingers evolution in the reference frame of the back of the plume for different capillary numbers Ca, i.e., for different thin film thickness δ. We find that the lateral width of the plume w_P remains very similar to the lateral droplet width $w = h - 2\delta$. The initial finger width is roughly proportional to the strata thickness $(h - \varepsilon)/2$ and, as the flow rate ratio φ decreases, fingers become thicker. However, for a given φ, the finger thickness decreases over time to conserve mass. When $\delta \approx 0$, the plume fills the entire channel (Fig. 10a) and strata fully detach from the walls. In this case, secondary fingers are observed to grow from the primary finger tips due to the recirculation vortices produced at the back of the translating droplet. In this example, we suspect the presence of diffusion effects as indicated by the blur in the miscible interface. For modest δ, the plume is separated from the walls by a thin film (Fig. 10b) and, for large δ, the plume is convected within the high-viscosity fluid (Fig. 10c). In this case, a droplet can initiate the opening of strata in its trail (Fig. 10c – top) and the high-viscosity fingers can buckle (Fig. 10c – bottom). Incidentally in this example, the film thickness δ is larger compared to data shown in Fig. 6a because the droplet size $d < 2h$.

Overall, the presence of finger indicates an increase of the miscible interface that enhances mixing between the low- and high-viscosity fluids. This mechanism appears more effective for large ε, i.e., when the high-viscosity fluid is slowly injected into the device, as well as when the droplet emission frequency is large compared to the stratification healing period.

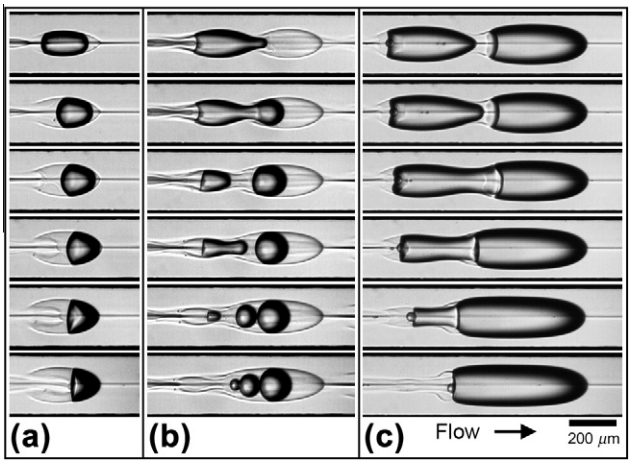

Fig. 11. Time-series of a small droplet dynamics in highly viscous stratifications, viscosity ratio $\chi = 1/1057$, Ca ≈ 1.9, $\varphi \approx 0.7$. (a) Droplet deformation in a cavity filled with low-viscosity fluid ($\Delta t = 10$ ms). (b) Multiple droplet snap-offs through a viscous constriction ($\Delta t = 2$ ms). (c) Coalescence between two daughter droplets ($\Delta t = 2$ ms).

5.3. Formation of low-viscosity conduits

The flow regimes associated with extremely small viscosity ratios ($\chi = 1/1057$) offer the opportunity to examine a variety of intriguing fluid phenomena. The high-viscosity matrices act as adjustable soft walls and induce droplet deformation, breakup, and coalescence (Fig. 11). The large slip ratio between streams facilitates the formation of channels inside the slow moving viscous medium. In addition, since the system is in partial non-wetting condition, we also find instances where the last daughter droplet sticks to the walls near the entrance of the stratified field. This droplet is then progressively displaced into the stratifications yielding arrays of very small droplets. For $\varepsilon/h \ll 1$, we observe cases where the low-viscosity fluid surpasses a small droplet and creates a cavity in its front (Fig. 11a). Deformable cavities can produce constrictions enabling the multiple snap-off of droplets (Fig. 11b). Another example of interaction between droplets and soft walls consists in the low-viscosity fluid invasion of closed strata between two consecutive daughter droplets that leads to their coalescence (Fig. 11c). Finally, asymmetrical deformation of stratifications are found for large flow rate ratio $\varphi > 50$. In this case, a droplet can channel through strata by deforming only the top layer and leaving the bottom layer relatively unchanged.

6. Conclusions

In this work, we study the hydrodynamic coupling between droplets and viscous stratifications using a square microchannel with two focusing sections. A droplet is essentially pushed parallel to flowing strips of different viscosities in a square duct. The large difference in velocity between parallel streams produces a variety of dynamics. Experiments are conducted with four stratification viscosities covering three decades in viscosity ratio for the separated flow.

We investigate the formation and morphology of stable viscous stratifications in a square microchannel. The results indicate that the viscous contributions to the system scale as $\chi^{1/2}$. The conditions for droplet breakup in a heterogeneous flow field are then analyzed. We find that a high-viscosity fluid can be used to fragment droplets into a controllable number of daughter droplets at low speed. A phase-diagram is proposed where the size of the mother droplet d_0/h is plotted as a function of a modified capillary number based on the geometric mean of the viscosity coefficients of the low- and high-viscosity fluids. The size of the first droplet is found to depend solely on the flow rate ratio φ for small viscosity ratios $\chi \leqslant 10^{-1}$. The difference in size between the first and the second droplet is related to the main capillary number and the film thicknesses between droplets and walls of the observation channel. The average droplet velocity is compared with the superficial multiphase flow velocity as a function of the capillary number and shows good agreement with previous theoretical work. We also examine the path of a droplet across viscosity stratifications. The closing of strata in front of the droplet and the formation of a plume at the back of the last daughter droplet are observed. The average velocity between the droplet and the plume is measured from high-speed movies and the formation and evolution of viscous fingers from the edges of high-viscosity matrices are discussed. Finally, we report the formation of low-viscosity fluid conduits in high-viscosity medium and the concept of soft high-viscosity walls is examined.

Overall, this study examines the possibility to probe novel multiphase flow scenarios using microfluidic devices. A difficulty in miniaturized fluid systems consists in systematically establishing transient flows, such as the propagation and evolution of viscous fingers and plumes in microgeometries. Viscous-stratified flows provide a means to build heterogeneous velocity fields and manipulate dynamical structures convected at different speeds. This study characterizes the behavior of deformable fluid particles interacting with a structured medium. In particular, we show the possibility to post-process microfluidic emulsions by modifying the continuous phase as well as displace high-viscosity oil with a low-viscosity emulsion in microgeometries. Future work will focus on the influence of stratifications made with miscible fluids having different interfacial tensions with droplets. The emergence and control of transient fluid phenomena with continuous microflows are promising for the development of new materials.

Acknowledgement

This material is based upon work supported by the National Science Foundation under Grant No. CBET-0932925.

References

Aubin, J., Ferrando, M., Jiricny, V., 2010. Current methods for characterizing mixing and flow in microchannels. Chem. Eng. Sci. 65, 2065–2093.
Baroud, C.N., Gallaire, F., Dangla, R., 2010. Dynamics of microfluidic droplets. Lab Chip 10, 2032.
Batchelor, G.K., 1967. An Introduction to Fluid Mechanics. Cambridge University Press, New York.
Bertherton, F.P., 1961. The motion of bubbles in tubes. J. Fluid Mech. 10, 166.
Brouzes, E., Medkova, M., Savenelli, N., Marran, D., Twardowski, M., Hutchison, J.B., Rothberg, J.M., Link, D.R., Perrimon, N., Samuels, M.L., 2009. Droplet microfluidic technology for single-cell high-throughput screening. Proc. Natl. Acad. Sci. USA 106, 14195–14200.
Cao, Q., Ventresca, A.L., Sreenivas, K.R., Prasad, A.K., 2003. Instability due to viscosity stratification downstream of a centerline injector. Can. J. Chem. Eng. 81, 913–922.
Cao, Q., Sarkar, K., Prasad, A.K., 2004. Direct numerical simulation for two-layer viscosity-stratified flow. Int. J. Multiphase Flow 30, 1485.
Che, Z., Nguyen, N.-T., Wong, T.N., 2011. Hydrodynamically mediated breakup of droplets in microchannels. Appl. Phys. Lett. 98, 054102.
Christopher, G.F., Anna, S.L., 2007. Microfluidic methods for generating continuous droplet streams. J. Phys. D: Appl. Phys. 40, R319.
Crowe, C.T., 2006. Multiphase Flow Handbook. CRC Press, Boca Raton.
Cubaud, T., 2009. Deformation and breakup of high-viscosity droplets with symmetric microfluidic cross flows. Phys. Rev. E 80, 026307.
Cubaud, T., Mason, T.G., 2006. Folding of viscous threads in diverging microchannels. Phys. Rev. Lett. 96, 114501.
Cubaud, T., Mason, T.G., 2007. Swirling of viscous fluid threads in microchannels. Phys. Rev. Lett. 98, 264501.
Cubaud, T., Mason, T.G., 2008a. Capillary threads and viscous droplets in square microchannels. Phys. Fluids 20, 053302.
Cubaud, T., Mason, T.G., 2008b. Formation of miscible fluid microstructures by hydrodynamic focusing in plane geometries. Phys. Rev. E 78, 056308.

Cubaud, T., Mason, T.G., 2009. High-viscosity fluid threads in weakly diffusive microfluidic systems. New J. Phys. 11, 075029.
d'Ocle, M., Martin, J., Rakotomalala, N., Salin, D., Talon, L., 2008. Pear and mushroom instability patterns in two miscible fluids' core annular flows. Phys. Fluids 20, 024104.
Gañán-Calvo, A.M., 1998. Generation of steady liquid microthreads and micro-sized monodisperse sprays in gas streams. Phys. Rev. Lett. 80, 285–288.
Gondret, P., Rabaud, M., 1997. Shear instability of two-fluid parallel flow in a Hele-Shaw cell. Phys. Fluids 9, 3267.
Guillot, P., Panizza, P., Salmon, J.B., Joanicot, M., Colin, A., Bruneau, C.H., Colin, T., 2006. Viscosimeter on a microfluidic chip. Langmuir 22, 6438–6445.
Günther, A., Jensen, K.F., 2006. Multiphase microfluidic: from flow characteristics to chemical and material synthesis. Lab Chip 6, 1487–1503.
Guyon, E., Hulin, J.-P., Petit, L., Mitescu, C.D., 2001. Physical Hydrodynamics. Oxford University Press, New York.
Hickox, C.E., 1971. Instability due to viscosity and density stratification in axysymetric pipe flow. Phys. Fluids 14, 251.
Irimia, D., Geba, D.A., Toner, M., 2006. Universal microfluidic gradient generator. Anal. Chem. 78, 3472–3477.
Ismagilov, R.F., Stroock, A.D., Kenis, P.J.A., Whitesides, G., Stone, H.A., 2000. Experimental and theoretical scaling laws for transverse diffusive broadening in two-phase laminar flows in microchannels. Appl. Phys. Lett. 76, 2376.
Knight, J.B., Vishwanath, A., Brody, J.P., Austin, R.H., 1998. Hydrodynamic focusing on a silicon chip: mixing nanoliters in microseconds. Phys. Rev. Lett. 80, 3863–3866.
Köster, S., Angilè, F.E., Duan, H., Agresti, J.J., Wintener, A., Schmitz, C., Rowat, A.C., Merten, C.A., Pisignano, D., Griffiths, A.D., Weitz, D.A., 2008. Drop-based microfluidic devices for encapsulation of single cells. Lab Chip 8, 1110–1115.
Larsen, M.U., Shapley, N.C., 2007. Stream spreading in multilayer microfluidic flows of suspensions. Anal. Chem. 79, 1947–1953.
Lee, G.B., Chang, C.C., Huang, S.B., Yang, R.J., 2006. The hydrodynamic focusing effect inside rectangular microchannels. J. Micromech. Microeng. 16, 1024–1032.
Lee, C.Y., Chang, C.L., Wang, Y.N., Fu, L.M., 2011. Microfluidic mixing: a review. Int. J. Mol. Sci. 12, 3263–3287.
Leshansky, A.M., Pismen, L.M., 2009. Breakup of drops in a microfluidic T junction. Phys. Fluids 21, 023303.
Link, D.R., Anna, S.L., Weitz, D.A., Stone, H.A., 2004. Geometrically mediated breakup of drops in microfluidic devices. Phys. Rev. Lett. 92, 054503.
Ménétrier-Deremble, L., Tabeling, P., 2006. Droplet breakup in microfluidic junctions of arbitrary angles. Phys. Rev. E 74, 035303(R).
Neils, C., Tyree, Z., Finlayson, B., Folch, A., 2004. Combinatorial mixing of microfluidic streams. Lab Chip 4, 342–350.
Nguyen, N.-T., Wereley, S.T., 2006. Fundamentals and Apllications of Microfluidics. Artech House Inc., Norwood.
Pannacci, N., Bruss, H., Bartolo, D., Etchart, I., Lockhart, T., Hennequin, Y., Willaime, H., Tabeling, P., 2008. Equilibrium and nonequilibrium states in microfluidic double emulsions. Phys. Rev. Lett. 101, 164502.
Prat, L., Sarrazin, F., Tasseli, J., Marty, A., 2006. Increasing and decreasing droplets velocity in microchannels. Microfluid. Nanofluid. 2, 271.
Ratulowski, J., Chang, H.-C., 1989. Transport of gas bubbles in capillaries. Phys. Fluids A 1, 1642.
Selvam, B., Merk, S., Govindarajan, R., Meiburg, E., 2007. Stability of miscible core-annular flows with viscosity stratification. J. Fluid Mech. 592, 23–49.
Seo, M., Paquet, C., Nie, Z., Xu, S., Kumacheva, E., 2007. Microfluidic consecutive flow-focusing droplets generators. Soft Matter 3, 986–992.
Song, H., Chen, D.L., Ismagilov, R.F., 2006. Reactions in droplets in microfluidic channels. Andew. Chem. Int. Ed. 45, 7336–7356.
Squires, T.M., Quake, S.R., 2005. Microfluidics: fluid physics at the nanoliter scale. Rev. Mod. Phys. 77, 977–1026.
Tabeling, P., 2005. Introduction to Microfluidics. Oxford University Press Inc., New York.
Teh, S.Y., Lin, R., Hung, L.H., Lee, A.P., 2008. Droplet microfluidics. Lab Chip 8, 198–220.
Than, P.T., Rosso, F., Joseph, D.D., 1987. Instability of Poiseuille flow of two immiscible liquids with different viscosity in a channel. Int. J. Eng. Sci. 25, 189.
Wan, J., Bick, A., Sullivan, M., Stone, H.A., 2008. Controllable microfluidic production of microbubbles in water-in-oil emulsions and the formation of porous microparticles. Adv. Mater. 20, 3314.
Wang, W., Xie, R., Ju, X.J., Luo, T., Liu, L., Weitz, D.A., Chu, L.Y., 2011. Controllable microfluidic production of multicomponent multiple emulsions. Lab Chip 11, 1587–1592.
Wong, H., Radke, C.J., Morris, S., 1995. The motion of long bubbles in polygonal capillaries. Part 1. Thins films. J. Fluid Mech. 292, 71.
Wu, Z.G., Nguyen, N.T., 2005. Hydrodynamic focusing in microchannels under consideration of diffusive dispersion: theories and experiments. Sens. Actuat. B – Chem. 107, 965–974.
Yiantsios, S.G., Higgins, B.G., 1988. Linear stability of plane Poiseuille flow of two superposed fluids. Phys. Fluids 31, 3225.
Yih, C.S., 1967. Instability due to viscosity stratification. J. Fluid Mech. 27, 337.
Yu, H.S., Sparrow, E.M., 1969. Experiments on two-component stratified flow in a horizontal duct. J. Heat Transfer 91, 51.